J. Applied Membrane Science & Technology, Vol. 29, No. 2, August 2025, 169–192

Structural, Thermal, and Surface Properties of PVDF/Silica Aerogel Nanocomposite Membranes for Membrane Distillation Application

A. Abdoli[a], S. A. Hashemifard[a]*, M. Abbasi[a], T. Matsuura[b], A. Khosravi[a]

[a]Chemical Engineering Department, Gas and Petrochemical Faculty, Persian Gulf University, Bushehr 7516913817, Iran

[b]Department of Chemical and Biological Engineering, University of Ottawa, 161 Louis Pasteur St., Ottawa, ON, Canada K1N 6N5

Submitted: 31/5/2025. Revised edition: 27/7/2025. Accepted: 28/7/2025. Available online: 1/8/2025

ABSTRACT

This study addresses membrane distillation's key challenges - wetting and thermal inefficiency - by developing PVDF/silica aerogel nanocomposite membranes with optimized sublayer properties. We fabricated membranes with systematic variations in PVDF concentration (12-21%) and silica aerogel loading (1-3%), characterizing their structural and surface properties. FTIR analysis confirmed successful nanoparticle incorporation without altering PVDF chemistry. Porosity exhibited concentration-dependent behavior: increasing with silica at 12% PVDF, stable at 18%, and decreasing at 21% due to viscosity effects on phase separation. All nanocomposites showed reduced thermal conductivity, enhancing insulation. While skin layer hydrophobicity remained constant, silica migration significantly increased sublayer contacts angles (peak 130.6° for 18% PVDF/3% silica, 20% improvement over control). The 18% PVDF formulation demonstrated optimal balance, maintaining structural integrity while achieving high porosity (78.3%) and low thermal conductivity (0.048 W/mK). These results highlight two critical findings: (1) PVDF concentration dictates nanoparticle effects on membrane morphology, and (2) strategic silica incorporation simultaneously enhances sublayer hydrophobicity and thermal resistance without compromising mechanical stability. The study provides a design framework for MD membranes, demonstrating how sublayer engineering can mitigate wetting while improving thermal efficiency - crucial advancements for practical MD implementation.

Keywords: Sublayer, contact angle, hydrophobicity, thermal conductivity, silica aerogel nanoparticles, membrane distillation

1.0 INTRODUCTION

Fresh water is vital for the sustenance of human societies; however, natural water systems have been disrupted by domestic activities and excessive industrial usage. Consequently, the world is confronted with the issue of water resource scarcity, compounded by insufficient infrastructure for water conservation. The increasing population, pollution of surface and groundwater resources, unequal distribution of water, and drought have compelled numerous societies and nations to seek alternative sources of water supply. This situation has prompted many researchers to innovate desalination techniques from saline water to ensure the availability of freshwater in the future [1, 2]. Generally, desalination techniques can be categorized into two main groups: thermal methods and membrane

* Corresponding to: S. A. Hashemifard (email: salhashemifard@yahoo.com)
DOI: https://doi.org/10.11113/jamst.v29n2.321

methods [3]. Given that conventional thermal processes require substantial energy, advancements in technology have led to the predominance of membrane processes, which have largely replaced traditional thermal methods due to their reduced size, enhanced flexibility, suitability for both domestic and industrial applications, improved selectivity and ability to separate specific compounds, higher efficiency, and lower energy requirements [4].

One of the most promising technologies is the membrane distillation process. This process combines the advantages of contemporary membrane separation techniques with traditional distillation methods, which are used in various separation applications including petrochemicals, fuel refineries, agriculture, food industries, water recycling, and salt extraction [4, 5]. The membrane distillation process offers several advantages, including complete removal of non-volatile compounds, a lower operating temperature compared to conventional distillation methods, lower operating pressure compared to pressure-driven membrane separation techniques such as reverse osmosis and nanofiltration, and the ability to utilize low-grade heat sources. Nevertheless, membrane distillation has not yet been fully industrialized due to certain limitations. Key challenges associated with the MD process include membrane wetting and suboptimal thermal efficiency [6, 7]. The wetting of membrane pores during the MD process remains a significant challenge. To address this issue, two main strategies have been widely adopted: 1) enhancing the hydrophobicity of the membrane surface, and 2) minimizing the size of the membrane pores. Research conducted by Lu *et al*. suggests that increasing the hydrophobicity of the membrane surface is a more effective approach to prevent pore wetting than simply reducing pore size, as the latter may lead to decreased porosity and increased tortuosity of the membrane, ultimately leading to reduced vapor flux [8, 9].

Membrane distillation, in contrast to other membrane techniques, is known as a non-isothermal process that uses a hydrophobic porous membrane as a physical barrier to separate solutes from water. The main driving force of this process is the vapor pressure difference on both sides of the membrane, which arises from a temperature gradient. [10, 11]. During the MD process, mass and heat transfer occure simultaneously. Depending on the configuration of the MD system, the vapor condenses either inside or outside the module, thereby transferring the latent heat of vaporization from the hot feed side to the cold permeate water. Additionally, another aspect of heat transfer in the MD process involves heat that is transferred directly through the membrane matrix, utilizing conductive heat transfer due to the temperature difference on both sides of the membrane. Conduction of heat leads to heat loss, which should be minimized as much as possible. Conductive heat transfer is primarily affected by the characteristics of the membrane under specific conditions, which serves as the most important factor in evaluating the thermal efficiency of the membrane. Consequently, improving the membrane properties is essential to minimizing energy consumption. One method to enhance membrane properties is to incorporate nanoparticles into the polymer matrix. Among the hydrophobic nanoparticles that exhibit low thermal conductivity and can reduce heat loss from the polymer membrane matrix are

hydrophobic silica aerogel nanoparticles. Silica aerogels consist of 96% air and a substantial matrix containing 20-25% silicon dioxide. Silica aerogel possesses unique and advantageous useful properties for the fabrication of MD polymer composite membranes, including low thermal conductivity (0.017 – 0.021 $W.m^{-1}K^{-1}$), low density (0.003 – 0.05 $gr.cm^{-1}$), and high porosity (80% – 99.8%). The air trapped in the nano porous framework significantly inhibits heat conduction, as air has poor thermal conductivity compared to solids. In addition, the irregular and twisted solid backbone of the silica lattice disrupts phonon transport, further reducing thermal conductivity. Furthermore, incorporating of silica aerogel into the matrix of the MD polymer membrane can also enhance the membranes' resistance to wetting [8, 12].

Li *et al*. applied a polydimethylsiloxane (PDMS)/PVDF mixture containing different concentrations of silica aerogel nanoparticles onto a commercial PVDF membrane to enhance the membrane's hydrophobicity and increase the contact angle. At a nanoparticle concentration of 30%, the contact angle of the commercial PVDF membrane increased from 128.4 to 162.3[13]. Zhang *et al*. achieved a 1.5% reduction in the thermal conductivity of a flat sheet membrane by incorporating silica aerogel nanoparticles with a PVDF polymer matrix. Furthermore, by modifying the surface of the PVDF with silica aerogel nanoparticles, they accomplished a significant reduction in thermal conductivity by 45.27%. They concluded that PVDF/SiAG bilayer membranes exhibited superior performance in minimizing thermal conductivity compared to PVDF/SiAG mixed matrix membranes [14]. Deka *et al*. also utilized a PDMS/PVDF mixture with different concentrations of silica aerogel nanoparticles to enhance the hydrophobicity and increase the contact angle on the polyvinylidene fluoride-co-hexafluoropropylene (PVDF/HFP) nanofiber membranes. At a 30% concentration of nanoparticles, the contact angle of the commercial PVDF membrane increased from 118.6 to 170[15]. Li *et al*. incorporate different ratios of silica aerogel nanoparticles with PVDF polymer to diminish reduce the thermal conductivity of the membrane. At 3% concentration of silica aerogel nanoparticles, the thermal conductivity of the flat sheet membrane decreased from 0.111 $W.m^{-1}K^{-1}$ to 0.083 $W.m^{-1}K^{-1}$ [15]. Rezaei *et al*. investigated the effect of incorporating silica aerogel nanoparticles and PDMS on the surface and matrix of polycarbonate hollow fiber membranes through an experimental approach. The addition of silica aerogel nanoparticles to the polymer matrix had a minimal effect on enhancing the contact angle of the membrane. Overall, membranes that were coated with silica aerogel nanoparticles and PDMS showed increased flux [8]. Zhang *et al*. applied a coating of a blend of different percentages of silica aerogel nanoparticles (ranging from 1.2% to 4.8%) and PVDF onto PET substrates, which resulted in improved hydrophobicity and temperature resistance, and achieved higher flux compared to the pure membrane [2].

The main objective of this research is to develop and perform initial evaluation of PVDF-based nanocomposite membranes containing with silica aerogel nanoparticles, with the aim of enhancing their hydrophobicity, porosity, and thermal performance. These improvements are essential for the production of hollow fiber membranes intended for

membrane distillation applications. This study seeks to provide an effective solution for optimizing membrane performance by investigating how changing in polymer concentration and nanoparticle content affect the structural and functional properties of the membranes.

It is important to highlight that in membrane distillation processes, the various layers of the membrane serve distinct functions, each of which can significantly affect overall performance. In particular, the membrane sublayer—which is typically in contact with the permeate side. Despite its importance, the surface properties of this layer have often been overlooked in prior research. In this work, we specifically analyze the sublayer surface, using FTIR to assess its chemical characteristics and explore its microstructural features. Our results indicate that the sublayer surface can influence membrane performance in MD, especially regarding wetting resistance. Notably, the sublayer exhibited a high contact angle, which is considered a novel feature of the fabricated membranes. To further assess this property, the minimum pressure required for membrane wetting (LEP) was determined through a pure water flux test using a home made setup.

2.0 EXPERIMENTAL

2.1 Materials

Polyvinylidene fluoride (PVDF) polymer powder was purchased from Arkema France. N-Methyl-2-pyrrolidone (NMP), with a purity of 99.95%, along with lithium chloride (LiCl) salt and 96% ethanol, were obtained from Merk, Germany. Hydrophobic silica aerogel powder was procured from Pakan Atieh Company, Iran.

2.2 Preparation of the Polymer Solution for the Neat Membrane

Initially, a portion of the PVDF powder was dehydrated in an oven at 60°C for a duration of 24 hours. Subsequently, LiCl salt was added into the NMP solvent and stirred for one hour until complete dissolution of the salt was achieved. Then, PVDF powder was then added to the solution in three equal increments, and continuously stirred and mixed for 24 hours using a magnetic stirrer at a constant speed (400 rpm), which ensured consistent shear conditions during mixing. After achieving a homogeneous solution, the resulting mixture was allowed to rest for 24 hours to facilitate the removal of trapped air bubbles, after which the membrane casting process was performed via phase inversion process.

2.3 Preparation of the Polymer Solution for the Nanocomposite Membrane

To prepare the polymer solution of the nanocomposite membrane, after dehydrating the PVDF powder, silica aerogel nanoparticles were added to the NMP solvent based on the solid phase. After complete mixing, the resulting mixture was placed in an ultrasonic device for 2 hours to uniformly disperse the nanoparticles. Then, LiCl salt was added to the solution and the mixture was continuously stirred for 1 hour at a constant speed of 400 rpm to maintain a consistent shear stress and ensure homogeneous mixing. Subsequently, the PVDF polymer was added to the solution in several steps, and the resulting mixture was stirred until a uniform solution was obtained. In

order to improve the uniformity and eliminate any aggregation of nanoparticles, the final solution was again sonicated for 2 hours. Finally, the prepared solution was degassed for several hours and used for membrane casting. The components of each polymer solution and the code related to the membranes are shown in Table 1.

Table 1 Dope composition and codes related to flat sheet membranes prepared in this study

Membrane code	PVDF wt%	NMP/LiCl wt%	SiAG wt%
M12	12	85/3	-
M12-1	12	85/3	1
M12-2	12	85/3	2
M12-3	12	85/3	3
M18	18	79/3	-
M18-1	18	79/3	1
M18-2	18	79/3	2
M18-3	18	79/3	3
M21	21	76/3	-
M21-1	21	76/3	1
M21-2	21	76/3	2
M21-3	21	76/3	3

2,4 Flat Sheet Membrane Fabrication

To make flat sheet membranes a doctor blade mashine manufactured by Sepanta Polymer Sharif Company (Iran) was utilized. Initially, the blade clearance of the apparatus was adjusted to a predetermined thickness of 35 µm. Subsequently, the casting solution was applied to a glass substrate. The blade was then drawn across the solution at a fixed speed (controlled by the doctor blade system) to ensure a consistent shear stress rate, resulting in a smooth and uniform film surface. Immediately afterward, the flat glass containing the polymer film was submerged in a coagulation bath filled with water. To ensure the complete extraction of the solvent from the membranes, they were immersed in tap water for a duration of 24 hours. Finally, the membranes were air-dried at room temperature for one day.

3.0 CHARACTERIZATION TESTS

3.1 Contact Angle

The contact angle of the membranes was recorded and measured using a home-made goniometer. Initially, water droplets with a volume of 3-5 µm were dispensed onto the membrane surfaces via a syringe embedded in the device. Subsequently, images of the water droplets on the membrane surface were captured using a camera with suitable precision (CCD, Connika). The contact angle was then determined using image processing software (ij149-jre6-32). To reduce the percentage of experimental error,

several samples of each membrane and eight distinct locations on the membrane surface were selected for contact angle measurement, and their average was reported.

3.2 Atomic Force Microscopy (AFM) Surface Characterization

The surface morphology and roughness of the flat sheet membranes incorporated with silica aerogel nanoparticles were analyzed using Atomic Force Microscopy (AFM) (Bruker, Dimension Icon). Membrane samples were carefully cut into 5 × 5 mm² squares and securely mounted on AFM stubs. A 10 × 10 μm² scanning area was selected to ensure representative surface characterization while maintaining high resolution. The measurements were performed in tapping mode to minimize surface damage, using a silicon cantilever with a nominal tip radius of <10 nm. Surface roughness parameters, Rq (root mean square roughness), was extracted from the height profiles to quantitatively assess the influence of SiAG NPs on membrane topography.

3.3 Membrane Overall Porosity Test

To determine the overall porosity of the membranes, the fabricated membranes were initially placed in a sealed container filled with ethanol for one hour. After this period, the selected membrane was removed from the ethanol container. Then, the weight of the membranes in wet state was accurately recorded. The samples were subsequently dried in ambient air for 24 hours, and their weight was measured again. Ultimately, the total porosity of the membrane was calculated using Equation 1.

$$\varepsilon\,(\%) = \frac{(W_{wet} - W_{dry})/\rho_e}{(W_{wet} - W_{dry})/\rho_e + W_{dry}/c} \qquad (1)$$

In this study, the following parameters were defined: W_{wet} (weight of the wet membrane sample), W_{dry} (weight of the dry membrane sample), ρe (density of ethanol), and ρc (effective density of the composite membrane, calculated as the weight-averaged density of the polymer matrix and incorporated nanoparticles). The densities of the polymer PVDF, SiAG and ethanol are 1.78 g/cm^3, 0.08 g/cm^3 and 0.783 g/cm^3, respectively.

3.4 Liquid Entry Pressure

The resistance of membranes against the membrane wetting was examined using the Liquid Entry Pressure (LEP) test. Specifically, the liquid entry pressure is defined as the minimum pressure that causes the membrane to become wet, and it is calculated using Young-Laplace Equation (2).

$$LEP = -\frac{2\emptyset\gamma COS\theta}{r_{max}} \qquad (2)$$

The surface tension is denoted by γ, ϕ represents the geometric factor associated with the structure of the pores (for cylindrical pores, it equals 1), and θ indicates the contact angle between the membrane surface and the liquid.

To investigate the LEP test, the setup illustrated in Figure 1 was used. This device ascts as a means of measuring water flux through the membrane. Various methods have been proposed for estimating LEP; in this study, a pure water flux setup was utilized to determine the minimum pressure that causes wetting of the membrane. Consequently, to record the LEP, the pressure on the feed side, which in this case is pure water, was gradually increased by 0.5 bar at 15-minute intervals. The pressure was increased until the first drop of water was observed on the membrane surface. Ultimately, the observed

pressure was reported as the LEP. To increase measurement accuracy, the feed water flow was maintained constant at each pressure to allow water to flow and be observed on the permeate side. The water flow rate was set to 200 ml/min. It is noteworthy that the feed water was in contact with the membrane from the skin layer side.

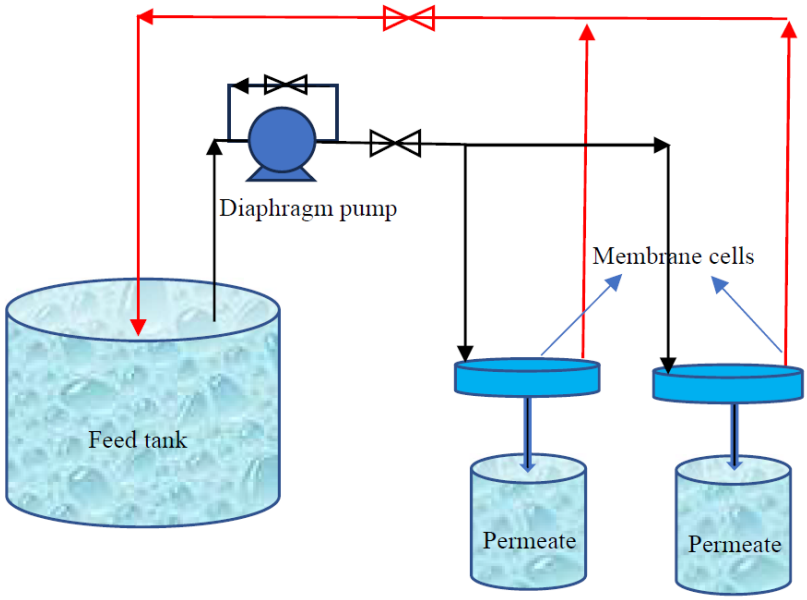

Figure 1 Schematic of LEP measuring instrument

3.5 Measurement of Thermal Conductivity of Membrane

This section of the study investigates the effect of incorporating silica aerogel nanoparticles, which have a low thermal conductivity even lower than that air, into the PVDF polymer matrix that has a thermal conductivity of 0.27 ($W.m^{-1}K^{-1}$). To evaluate the thermal conductivity of the produced membranes, a linear thermal conductivity device developed by Armfield (UK) was used. For this analysis, the samples were shaped into circles with a diameter of 25 mm and placed inside the thermal conductivity testing machine. Using a thin layer of superconducting paste film on both sides of the flat sheet membranes significantly reduced the air gap, thereby reducing measurement error. Given that the conductivity of the superconducting paste is significantly higher than that of the membrane, its resistance was deemed negligible. It should be noted that, since the measurement conditions for the membrane samples are almost the same, the relative conductivity of the membranes can be compared. As illustrated in Figure 2, the device consists of two separate hot and cold sections. The hot section is heated by an electric element, while the cold section is maintained at a constant temperature through a flow of tap water. The electrical heating power of the device's element was calibrated to a specific value. To achieve a stable condition, each membrane sample was allowed 60 minutes to reach a steady state before data were recorded. Ultimately, the thermal conductivity of each sample was determined using Fourier's law of thermal conductivity (Equation 3).

$$k = \frac{qL}{\Delta TA} \tag{3}$$

The thermal power, denoted as q (W), represents the heat transfer capability of the porous membrane, which is characterized by its thermal conductivity k ($W.m^{-1}K^{-1}$), the area of heat transfer of the samples A (m^2), the temperature difference across the two sides of the membrane ΔT (K), and the thickness of the membrane L (m) [8].

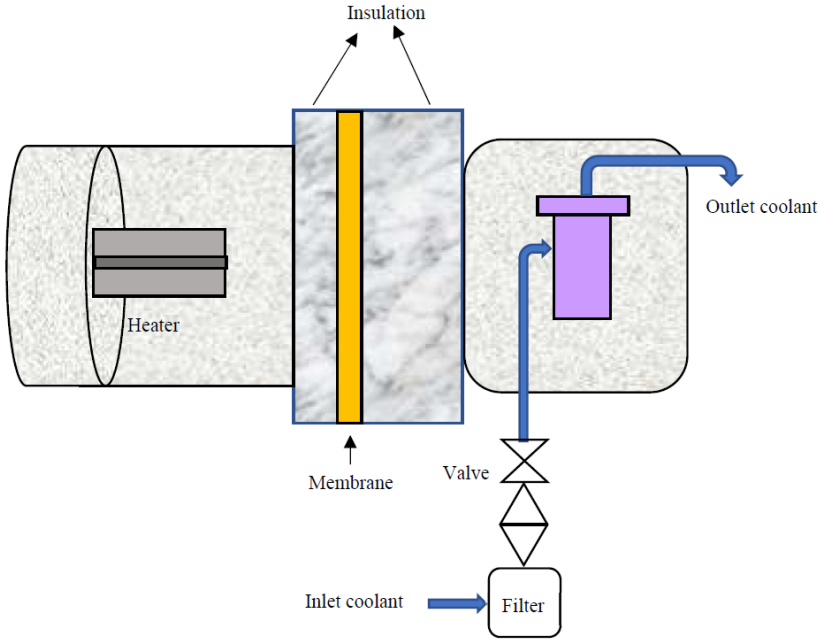

Figure 2 Schematic of heat conduction measuring instrument

3.6 FTIR Test

FTIR spectroscopy analysis was conducted using a Jasco FTIR spectrometer equipped with an ATR (Attenuated Total Reflectance) accessory. This technique provided surface-sensitive analysis of the membrane's chemical structure without requiring sample preparation. Spectra were collected over the 4000-400 cm^{-1} range to confirm the integrity of the PVDF polymer and to evaluate nanoparticle distribution between the skin layer and the substrat.

4.0 RESULTS AND DISCUSSION

4.1 Contact Angle

As a measure of the hydrophobicity index of the produced membranes, the contact angle with water was evaluated. The contact angle of both the skin layer and the sublayer were investigated by changing the ratio of silica aerogel nanoparticles in the PVDF polymer matrix. As shown in Figure 3a, the contact angle of the skin layer increased from 82.48 (for the neat M12 membrane) to a peak of 84.21 at a concentration of 3% for the M12-3 membrane. It can be concluded that incorporating silica aerogel nanoparticles into the PVDF polymer matrix did not significantly enhance the contact angle of the membrane's skin layer. Given that the skin layer is directly exposed to air, the rapid evaporation of the solvent during the phase separation process limits the nanoparticles' ability to migrate to the surface. As a result, most of the nanoparticles remain embedded within the polymer matrix, resulting in no significant changes in morphology or surface chemistry of the skin surface.

Conversely, analysis of the effect of incorporating silica aerogel nanoparticles, ranging from 1% to 3%, the PVDF polymer matrix showed significant changing in the contact angle of the membrane sublayer. The M12-1 membrane sublayer exhibited the highest contact angle of 120.9. This phenomenon occurs because the subslayer is directly in contact with the coagulation bath, resulting in a slower exchange between solvent and nonsolvent. Such conditions facilitate the migration of nanoparticles further towards the sublayer, or even their accumulation within it. Consequently, the presence of nanoparticles significantly affects the surface of the sublayer, leading to an increase in the contact angle.

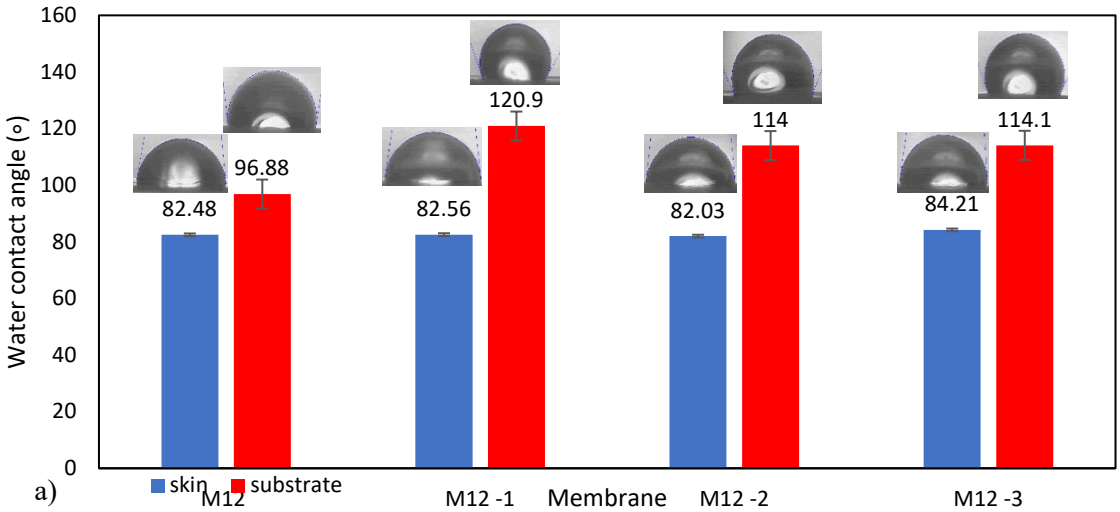

a)

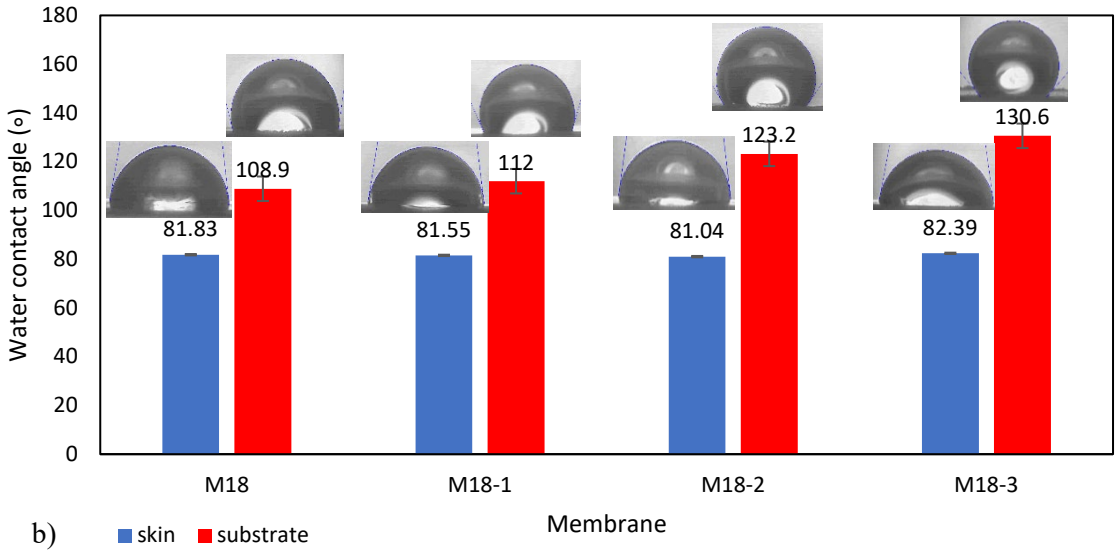

b)

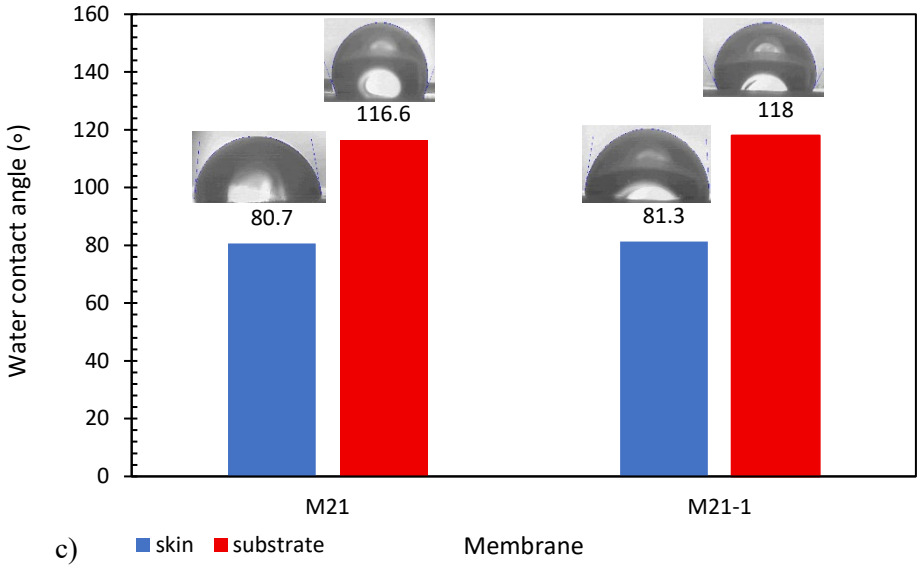

Figure 3 Effect of SiAG nanoparticle loading (%) on the water contact angle of the skin and sublayers in membarnes: a) membrane M12, b) membrane M18, and c) membrane M21

Figure 3b illustrates the investigation of changes in the contact angle for the M18 after adding 1% to 3% silica aerogel nanoparticles to the PVDF polymer matrix. It is obvious that with the addition of 3% silica aerogel nanoparticles, the contact angle of the membrane's skin layer increased from 81.83 to 82.39. As a result, the addition of silica aerogel nanoparticles from 1% to 3% to the PVDF polymer matrix had little effect on increasing contact angle of the M18 membrane's skin layer. Conversely, an analysis of the influence of adding silica aerogel nanoparticles from 1% to 3% to the PVDF polymer matrix revealed a significant effect on increasing of the contact angle of the membrane sublayer. The contact angle for the membrane sublayer increased from 108.9 for the unmodified M18 membrane to 130.6 for the M18-3 membrane.

As the polymer content increased to 21 wt%, membranes with 2 and 3 wt% silica aerogel nanoparticles developed severe surface heterogeneity and structural irregularities. This could be due to the increase in solution viscosity and the resulting aggregation of nanoparticles during the membrane casting process. These defects prevented proper membrane formation and made it impossible to perform some performance tests. In contrast, the M21-1 membrane had a uniform structure and adequate mechanical integrity for the tests. At this stage, the contact angle was measured for the neat M21 and M21-1 membranes. As can be seen in Figure 3c, with the loading of 1 wt% silica aerogel nanoparticles, the skin layer contact angle of the neat M21 membrane increased from 80.7 to 81.3, which can be said to be negligible. The sublayer contact angle also increased from 116.6 to 118 for the M21-1 membrane, which was not a significant increase. This observation is consistent with the results of previous studies. Zhang *et al*. increased the contact angle from 91 to 93 by adding SiO_2 nanoparticles to the membrane matrix which had no significant effect [16]. Afom *et al*. also reported that the contact angle of neat PVDF membrane increased from 75 to 75.5 by adding 0.5% silica aerogel nanoparticles. They also reported that

the contact angle barely reached 95 by increasing the silica nanoparticles to 10 wt% [17]. Li *et al*. also enhanced the contact angle of the membrane's skin layer from 81.8 to 106.3 by incorporating 3% silica aerogel nanoparticles into the PVDF polymer matrix [18]. Rezaei *et al*. further demonstrated that the addition of silica aerogel nanoparticles to the polycarbonate membrane's polymer matrix did not lead to a significant increase in the contact angle [8]. It can be inferred that in membranes with a high polymer content (18% and 21%), the increase viscosity limits the movement of nanoparticles towards the surface; consequently, a greater number of nanoparticles are distributed within the matrix's depth. Thus, at these higher percentages, the skin layer experiences less influence. Conversely, in the sublayer, the gradual development of the structure allows for better dispersion of nanoparticles on the surface.

As illustrated in Figures 3a, b, and c, all the fabricated membranes exhibited a higher contact angle on the sublayer compared to the skin layer. This observation leads to the conclusion that during the membrane formation process via the phase inversion method, the skin layer's surface, due to direct exposure to air and increased evaporation of the solvent, along with the rapid and direct interaction with water as a non-solvent, facilitates the movement of superhydrophobic silica aerogel particles. These particles tend to quickly separate from the water and migrate towards the sublayer, resulting in their accumulation. Consequently, the membrane's surface, or skin layer, remains devoid of these particles, while the underlying surface, or sublayer, becomes enriched with nanoparticles. This difference in surface conditions relative to the sublayer within the coagulation bath, particularly in the presence of nanoparticles, is a significant factor contributing to the observed increase in the water contact angle of the sublayer when compared to the skin layer. Furthermore, as illustrated in Figures 3a, b, and c, the contact angle of the skin layer of the nanocomposite membrane decreased with increasing polymer concentration. These findings indicates that, along with the percentage of nanoparticle loading, the quantity of PVDF polymer present in the casting solution plays a crucial role in influencing the contact angle. This phenomenon may be attributed to the reduction in polymer concentration, which results in an increase in void spaces, thereby increasing the number of pores that absorb air, potentially hindering water diffusion at the three-phase interface. As a result, a greater quantity of nanoparticles can be accommodated on the surface. As a result, since nanoparticles are inherently hydrophobic, an increased presence of these particles on the membrane surface increasing the contact angle, which is consistent with the research conducted by Li *et al*. They similarly observed an increase in the contact angle with decreasing polymer concentration [18]. The contact angle for silica aerogel nanoparticles is shown in Figure 4.

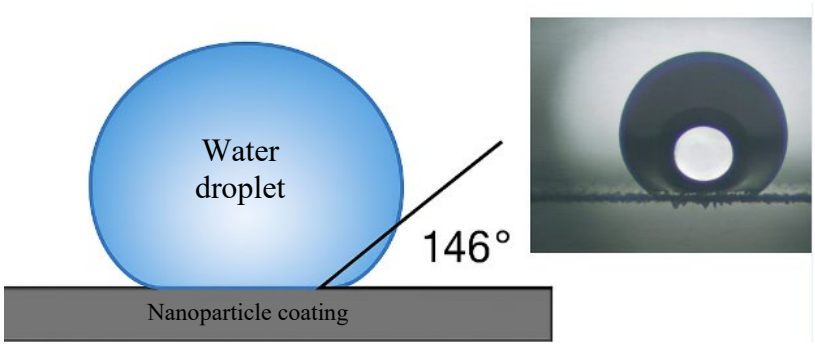

Figure 4 Image of the contact angle of a water droplet on a surface modified hydrophobic silica aerogel nanoparticles

4.2 Topology of the Membranes Surfaces

The AFM images of the upper surface of the composite membrane sare shown in Figure 5. The AFM analysis of the composite membranes revealed significant variations in surface roughness (Ra) depending on PVDF concentration and silica nanoparticle loading. The M12 series (12% PVDF) showed that increasing silica NP content from 1% to 3% reduced roughness from 36.43 nm to 29.61 nm, suggesting improved nanoparticle dispersion at higher loadings in this polymer matrix. In contrast, the M21 series (21% PVDF) exhibited different behavior: while M21-1 (1% silica NPs) maintained moderate roughness (29.61 nm), M21-3 (3% silica NPs) displayed dramatically increased roughness (69.59 nm).

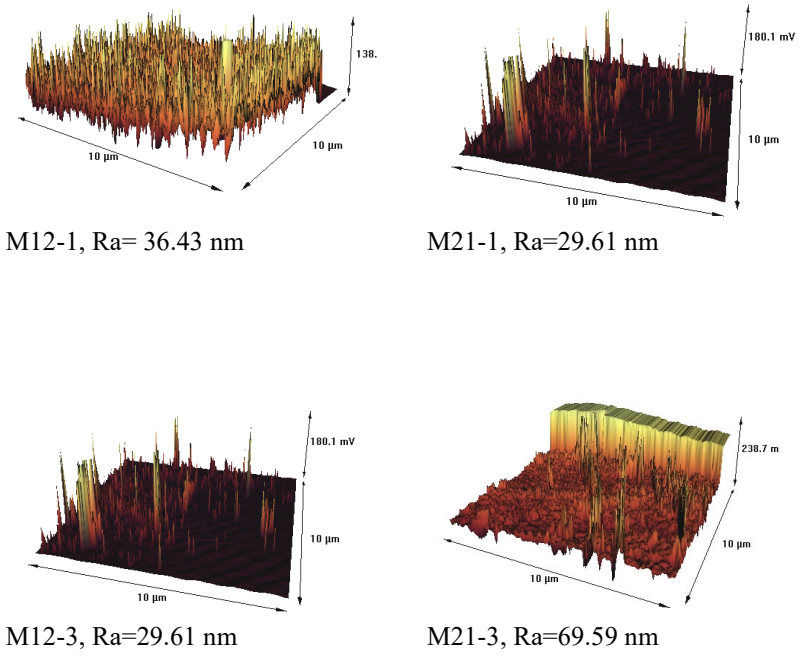

M12-1, Ra= 36.43 nm M21-1, Ra=29.61 nm

M12-3, Ra=29.61 nm M21-3, Ra=69.59 nm

Figure 5 the AFM image of the upper surface of the fabricated composite membranes

This sharp rise indicates potential nanoparticle aggregation or phase separation occurring at higher PVDF concentrations, where increased polymer viscosity may hinder uniform NP distribution. The results demonstrate that surface morphology is strongly influenced by the interplay between polymer content and nanofiller loading, with optimal uniformity achieved at 12% PVDF with 3% silica NPs. These roughness variations could significantly affect membrane performance characteristics such as permeability and fouling resistance, suggesting the need for careful optimization of composition parameters for specific applications.

AFM images depicting the lower surface topography of the composite membranes are presented in Figure 6.

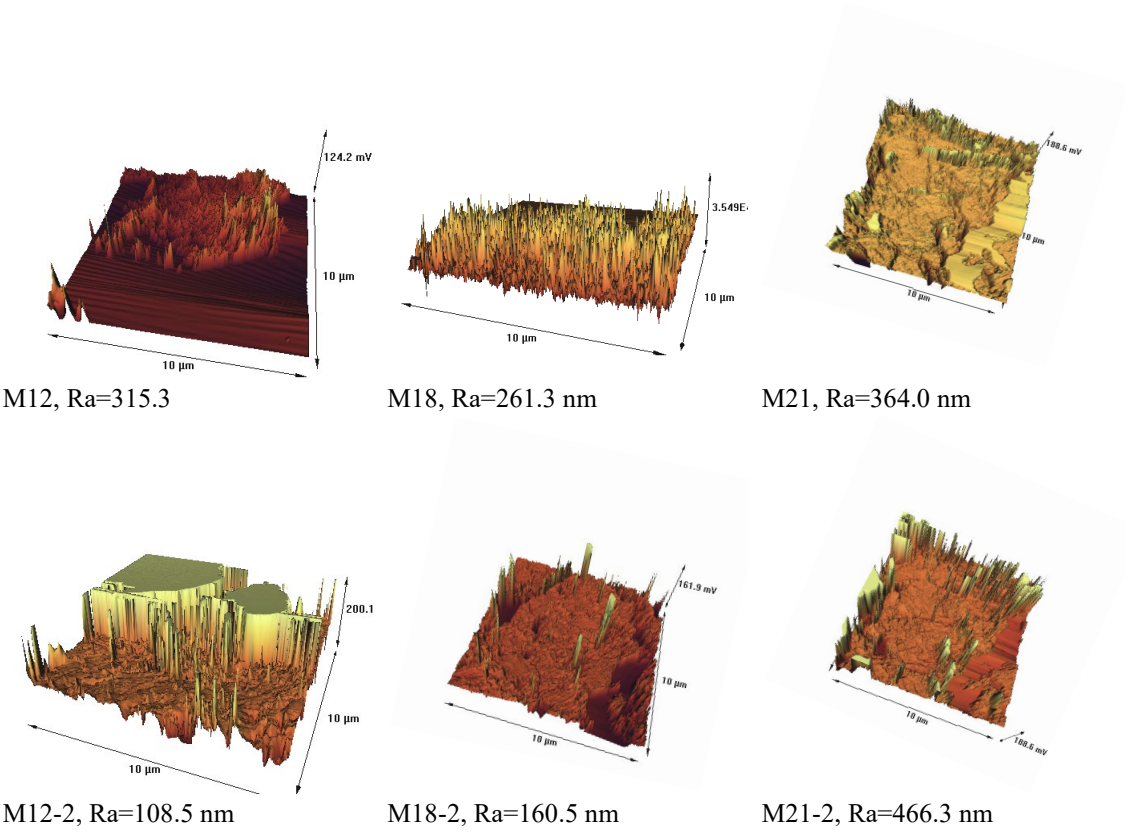

M12, Ra=315.3 M18, Ra=261.3 nm M21, Ra=364.0 nm

M12-2, Ra=108.5 nm M18-2, Ra=160.5 nm M21-2, Ra=466.3 nm

Figure 6 the AFM image of the lower surface of the fabricated composite membranes

The AFM measurements of the lower membrane surfaces revealed significantly higher roughness values compared to the upper surfaces, confirming the expected migration of silica nanoparticles toward the bottom layer during membrane formation. This phenomenon was further supported by contact angle measurements, which showed higher values for the lower surfaces due to their enhanced roughness and nanoparticle enrichment. The M12 series exhibited a substantial decrease in roughness from 315.3 nm (M12) to 108.5 nm (M12-2) with silica NP incorporation, suggesting that even a modest nanoparticle loading (2%) helped moderate surface irregularities. Similarly, the M18 membranes showed a roughness reduction from 261.3 nm (M18) to 160.5 nm (M18-2),

reinforcing the trend that silica NPs improve lower surface uniformity at intermediate PVDF concentrations. However, the M21 series displayed an opposite behavior, with roughness increasing dramatically from 364.0 nm (M21) to 466.3 nm (M21-2) upon NP addition. This suggests that at higher PVDF content (21%), nanoparticle migration may lead to severe aggregation or phase separation, exacerbating surface heterogeneity. The results highlight that while silica NPs generally promote smoother lower surfaces in lower PVDF concentrations (12–18%), their effect becomes detrimental at higher polymer content, likely due to altered polymer-NP interactions and sedimentation dynamics during membrane casting. These findings correlate well with the observed hydrophobicity trends, where increased roughness contributed to higher contact angles on the nanoparticle-enriched lower surfaces.

4.3 Overall Membrane Porosity

Membranes with higher porosity offer more surface area for vapor transfer, leading to enhanced flux. Reports indicate that the porosity of MD membranes typically ranges from 20% to 85% [19]. The overall porosity of all prepared membranes was evaluated and compared. As shown in Figure 5, regardless of the amount of silica aerogel nanoparticles, an increase in polymer concentration resulted in a reduction of membrane porosity. This is especially evident with the increasing polymer concentration from 12% to 18%. Furthermore, as depicted in Figure 7, the overall porosity of the M12 membrane increased with the addition of silica aerogel nanoparticles to the polymer matrix. However, with the same amount of silica aerogel nanoparticles, specifically 1, 2, and 3 wt%, no significant changing was observed in the overall porosity of the M18 membrane. Notably, the overall porosity of the M21 membrane exhibited a decline. It can be inferred that as the polymer concentration in the solution increases, the solution becomes more concentrated, resulting in a decrease mobility of the polymer chains. Consequently, during the coagulation process, non-solvent penetration into the polymer film occurs at a slower rate, and the phase separation process takes longer, ultimately resulting in a denser structure characterized by smaller pore sizes and, consequently, reduced porosity. Membranes derived from high concentration polymer solutions typically have a “spongy” and denser structure, in contrast to membranes with lower polymer percentages that exhibit a finger-like structure and higher porosity. Naeem *et al*. also determined that by analyzing various concentrations of PEI polymer ranging from 13 to 16 wt%, the pore size and porosity of the membrane decreased with increasing polymer concentrations [20].

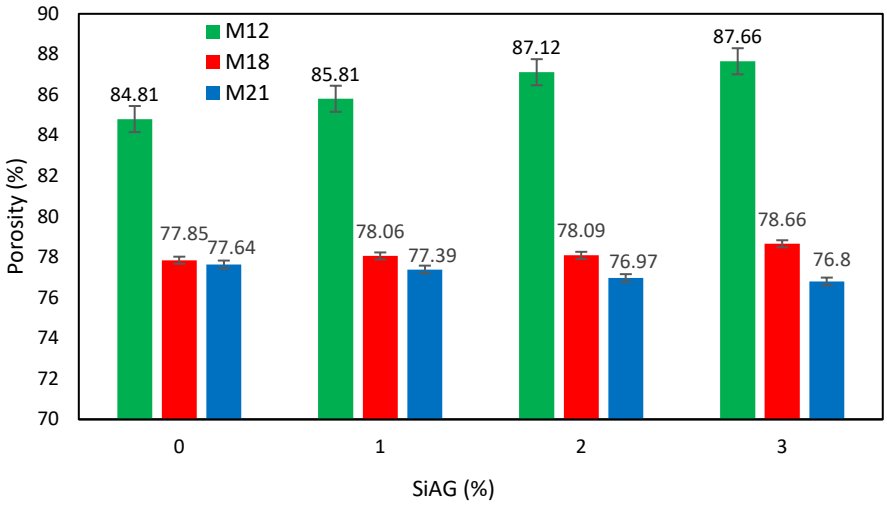

Figure 7 The effect of SiAG (%) loading on the overall porosity M12, M18, M21 membranes

4.4 Flux and Liquid Entry Pressure

The results of the pure water flux and liquid entry pressure tests are illustrated in Figures 8a and 8b. The point at which each line intersects the pressure axis represents the liquid entry pressure, which indicates the minimum pressure required for membrane wetting. The linear equations representing the flux of each membrane are depicted in the figures. By setting the flux value to zero in these equations, the LEP values were derived (refer to Table 2). It is evident that as the concentration of silica aerogel nanoparticles increases, the LEP diminishes from 2.66 to 1.43 bar for the M12 membrane and from 4.85 to 4.11 bar for the M18 membrane, respectively. The values recorded by the pressure gauge are also presented in Table 2. A strong correlation is observed between the values obtained from the pressure gauge and calculated values. According to Laplace's equation, the LEP for a constant liquid is influenced by two factors: the contact angle and the size of the membrane pores. Given that there was no notable increase in the contact angle of the membrane skin layer with the addition of silica aerogel nanoparticles, the reduction in liquid entry pressure can likely be attributed to the enlargement of the membrane pore size [8]. The size of the membrane pores is a critical determinant of membrane performance [21]. By reducing the polymer concentration, a relatively higher contact angle was achieved, albeit with a lower liquid entry pressure. In research conducted by Li *et al*., a similar trend was observed where a higher contact angle and a lower liquid entry pressure were recorded for nanocomposite membranes with decreased polymer concentration [18]. Additionally, a study by Rezaei *et al*. found that the LEP for nanocomposite membranes containing nanoparticles in the membrane matrix was lower than that of membranes modified with silica aerogel nanoparticles; however, in both cases, membranes that were either combined or modified with nanoparticles exhibited higher liquid entry pressures [8].

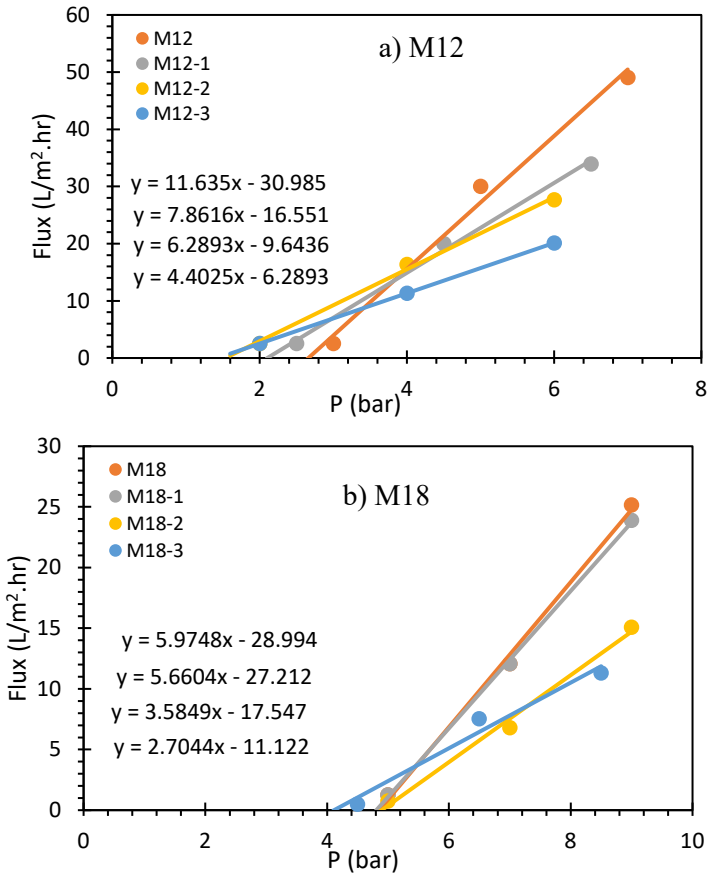

Figure 8 Effect of SiAG nanoparticle loading (%) on the water flux of membranes a) membrane M12 and b) membrane M18

Table 2 The LEP results of prepared flat sheet membranes

Membrane	M12	M12-1	M12-2	M12-3	M18	M18-1	M18-2	M18-3
Calculated LEP (barg)	**2.66**	**2.11**	**1.51**	**1.43**	**4.85**	**4.81**	**4.89**	**4.11**
Measured LEP (barg)	**3.0 ±0.2**	**2.5±0.2**	**2.0±0.2**	**2.0±0.2**	**5.0±0.2**	**5.0±0.2**	**5.0±0.2**	**4.5±0.2**
Pure water flux (LMHbar)	**11.6±0.5**	**7.9±0.5**	**6.3±0.5**	**4.4±0.5**	**6.0±0.5**	**5.7±0.5**	**3.6±0.5**	**2.7±0.5**
Thickness (mm)	**0.711±0.01**	**0.717±0.01**	**0.796±0.01**	**0.825±0.01**	**0.148±0.01**	**0.149±0.01**	**0.149±0.01**	**0.158±0.01**

The incorporation of silica aerogel nanoparticles resulted in an increase in the thickness of the M12 and M18 membranes. According to Li *et al.*, this phenomenon may be attributed to the increase in mass within the membrane matrix (the solid component of the membrane). This claim seems to be valid. Furthermore, it appears that silica aerogel nanoparticles may significantly contribute to reducing membrane shrinkage during the drying phase. Additionally, the introduction of silica aerogel nanoparticles into the membrane matrix can facilitate the formation of free space within the membrane's structure. Moreover, the hydrophobic nature of silica aerogel particles enhances porosity by creating voids around the nanoparticles. The cumulative effect of these processes can lead to an increase in membrane thickness. The thickness of the membrane is crucial in the membrane distillation process, as an increase in thickness results in a reduction of

vapor flux due to the longer mass transfer pathway [8, 22]. Notably, as the amount of silica aerogel nanoparticles increases, there is a corresponding decrease in pure water flux. This reduction may be related to the increased thickness of the membrane. It may also indicate a reduction in the average pore size of the membrane. This observation is particularly intriguing, because it coincides with an increase in the largest pore size, which controls the membrane LEP.

4.5 Thermal Conductivity Results

The findings from the evaluation of the thermal conductivity of the synthesized membranes, which are affected by the amount of nanoparticles, are shown in Figure 9.

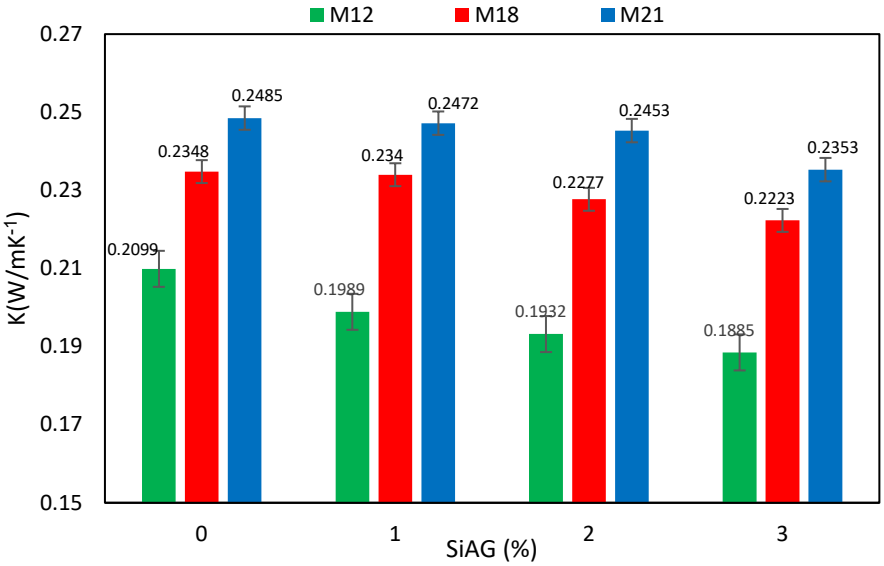

Figure 9 The effect of SiAG (%) loading on the thermal conductivity M12, M18, M21 membranes

Both membrane thickness and thermal conductivity can significantly effect the thermal efficiency of the membrane distillation (MD) process. increasing membrane thickness reduces the system's efficiency in terms of flux. Conversely, reducing the membrane thickness, which increases heat loss within the system, leads to a decrease in the driving force generated by the temperature difference, ultimately resulting in lower thermal efficiency. Furthermore, a membrane matrix with lower thermal conductivity contributes to reduced heat loss, thereby enhancing thermal efficiency [8]. As shown in Figure 9, the overall thermal conductivity increseas with increasing polymer concentration, which is attributed to the reduction in porosity, which acts as an insulating component of the membrane structure. However, the incorporation of silica aerogel nanoparticles into the M12, M18, and M21 membranes resulted in a reduction of thermal conductivity from 0.2099 to 0.1885, from 0.2348 to 0.2223, and from 0.2458 to 0.2353, representing a reduction of 7.2%, 5.3%, and 4.3% respectively. In this context, Li *et al*. noted that the addition of silica aerogel nanoparticles at a concentration of 0.5% to the PVDF polymer matrix did not result in a significant change in thermal conductivity. When nanoparticles were added to the polymer membrane matrix up to 3%, the thermal conductivity of

the PVDF flat sheet membrane decreased from ($W.m^{-1}K^{-1}$ 0.111) to ($W.m^{-1}K^{-1}$ 0.083) [18]. Similarly, Rezaei *et al*. at SMTRG observed a reduction in the thermal conductivity of the membrane from ($W.m^{-1}K^{-1}$ 0.2415) to ($W.m^{-1}K^{-1}$ 0.2411) by incorporating 0.5% silica aerogel nanoparticles into the polycarbonate polymer matrix, which exhibited minimal change and remained almost constant [8]. It is important to note that, in addition, the addition of aerogel nanoparticles resulted in a decrease in the membrane thermal conductivity, which could increase the membrane's resistance to thermal efficiency loss during membrane distillation. By minimizing conductive heat loss across the membrane, a better thermal gradient is maintained, which is essential for stable vapor transfer and overall process efficiency.

The findings from the thermal conductivity investigation of membranes created with different polymer percentages showed that the incorporation of nanoparticles has a significant effect on membranes with lower polymer concentrations, and lead to a further reduction in thermal conductivity. This effect is primarily attributed to the increasead porosity, which allows for a greater amount of air to be trapped in the membrane structure; given that the thermal conductivity of air (0.025 $W.m^{-1}K^{-1}$) is considerably lower than that of polymer (0.027 $W.m^{-1}K^{-1}$) [12]. In contrast, membranes with 12% polymer showed the lowest thermal conductivity, can be attributed to their highest porosity.

4.6 FTIR Analysis of the Membranes' Skin Layer

As shown in Figure 10a and 10b, the neat membranes exhibit a peak at 1402 (CH2), that is related to the bending vibration of the methylene group, a feature commonly found in aliphatic polymers such as PVDF. Additionally, the peaks at 1274 (C-F bending/stretch) and 1168 (C-F stretching) represent the C-F bond, which is often observed in the α-phase structure of PVDF, while the significant stretching vibration associated with the C-F bond is particularly characteristic of the β-phase. The peak at 1072 (C-C or C-F vibration) indicates the combined movements of the carbon chain with fluorine. The peak at 879 (CF2 deformation) reflects the β-phase crystalline structure in PVDF, while the peak at 838 (CF2 wagging or rocking) can represent either the α or β phase, depending on the intensity and position. The peaks identified in the neat membranes are fully consistent with the structural characteristics of PVDF. The absence of peaks at 1660 or 2900 indicates that there is no residual NMP solvent present in the membrane structure. Furthermore, LiCl did not show a distinct peak. The peak at 3727 in the M12-1 membrane indicates the presence of partial absorbed moisture or residual OH groups. Peaks at 3018 and 2979 still originate from the PVDF structure and NMP solvent. The incorporation of hydrophobic nanoparticles did not change the polymer bonds, as there was no direct interaction between the C-H groups and the silica surface. The peak with an intensity of 1072 is associated with the Si-O-Si structure. Its relatively high intensity indicates that, despite the modification of the nanoparticle surface with hydrophobic groups, the SiO_2 structural core remains active and discernible in the spectrum. The peak at 472 represents the specific Si-O bending signal, which persists despite the hydrophobic nature of silica. The presence of six peaks in the M18-1 membrane in the broad

range from 3723 to 3527 clearly indicates the existence of OH stretching bands, the potential cause of which has been previously discussed. The significant intensity of peaks 3018 and 2979 in this sample indicates that the fundamental structure remains entirely intact. The reduction in the intensity of the peak 1400 with increasing polymer concentration, compared to the M12-1 sample, may be attributed to the possibility that the nanoparticles have suffered damage from the PVDF crystal structure. In addition, the decrease in the intensity of peak 1170 relative to M12-1 sample could indicate that the crystal structure has been somewhat influenced by the increase in polymer concentration and the incorporation of SiAG. The lower intensities observed at peaks 838 and 877 may result from a decline in crystallinity, likely due to the increased effect of the nanoparticle on the PVDF chains at high concentrations. In summary, in M18-1 sample, the hydrophobic nanoparticle had a more significant influence on the disruption of the PVDF crystal structure compared to M12-1 sample. The intensities of peaks 1072, 472, and 507 reflect the effective presence of the nanoparticle. Additionally, while the fundamental structure remains intact, there is a reduction in crystallinity, which could potentially influence the mechanical properties or porosity. An increase in nanoparticle content to 2% in the M12-containing membrane led to a slight reduction in crystallinity (especially at peaks 1172 and 877), however the overall structure of PVDF was still well preserved. The high intensity of the silica peaks (1072 and 472) indicates effective dispersion of the nanoparticles, without significantly reducing the PVDF signals. Given that PVDF constitutes a lower percentage (12%) in this membrane, the nanoparticles have more space to disperse and interact with the polymer matrix, which may have resulted in a slight decrease in chain order. In the M18-2 membrane, the prominence of the silica peaks (1079, 472, 507) effectively indicates the existence of silica aerogel nanoparticles in the matrix, with their high intensity reflecting an appropriate distribution and efficient dispersion of these nanoparticles throughout the membrane.

Overall, increasing the proportion of silica aerogel nanoparticles from 1% to 2% apparently resulted in further disruption of the crystalline structure of PVDF; however, the nanoparticles were well-distributed in the matrix and did not cause significant interference with the original PVDF bands. The reduced intensity of the peaks at 1170 and 838 in the M12-3 membrane indicates that the incorporation of nanoparticles led to a slight decrease in crystallinity. It is possible that the nanoparticles are still embedded and not prominently visible on the surface. No significant change were obsorved compared to the M12-1 and M12-2 samples. Despite the increased amount of nanoparticles, their distribution and location (likely buried) appear to have a greater impact than their net amount. The peaks at 1172 and 1072 in the M18-3 membrane indicate the impact of nanoparticles on the PVDF polymer structure. These peaks are more prominent in the nanoparticle nanocomposite membranes relative to the neat membranes, potentially due to the presence of nanoparticles on the polymer surface or interactions with the silica present. Peaks at 1400 and 1274, associated with the α phase, remain clearly visible in this membrane; however, a slight reduction in the intensity of the 1400 peak, especially in membranes containing 18% PVDF, may be attributed to the effect of nanoparticles on the crystal structure [23].

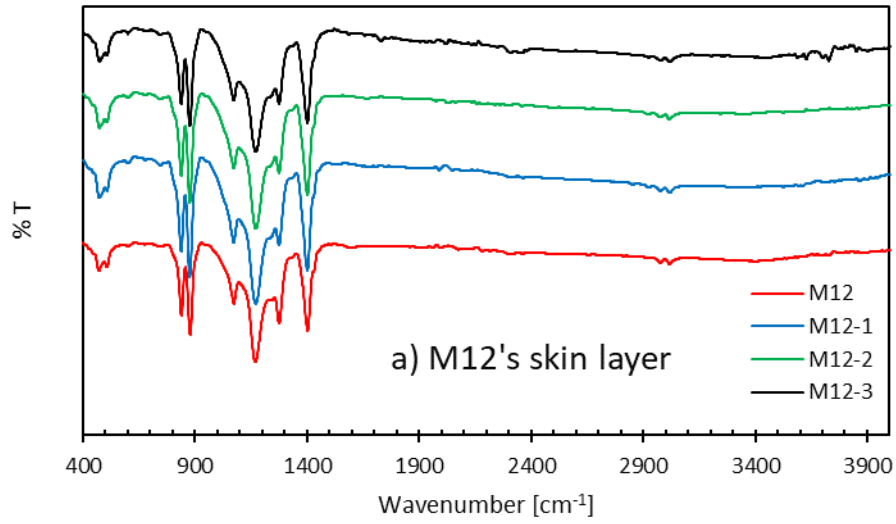
% T
M12
M12-1
M12-2
M12-3
a) M12's skin layer
400
900
1400
1900
2400
2900
3400
3900
Wavenumber [cm-1]

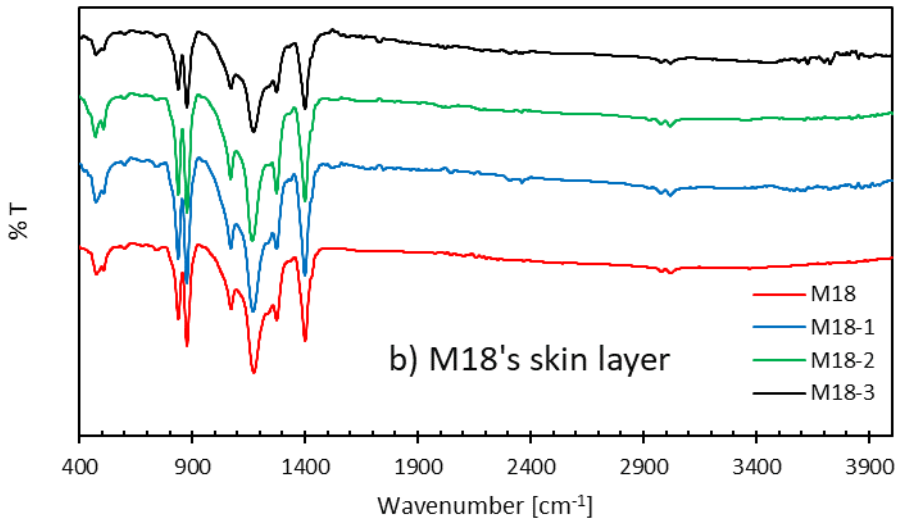
% T
M18
M18-1
M18-2
M18-3
b) M18's skin layer
400
900
1400
1900
2400
2900
3400
3900
Wavenumber [cm-1]

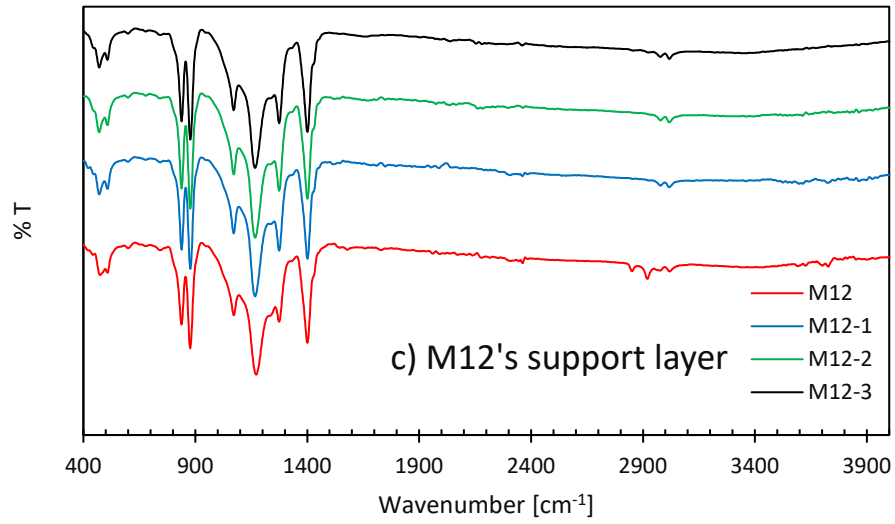
% T
M12
M12-1
M12-2
M12-3
c) M12's support layer
400
900
1400
1900
2400
2900
3400
3900
Wavenumber [cm-1]

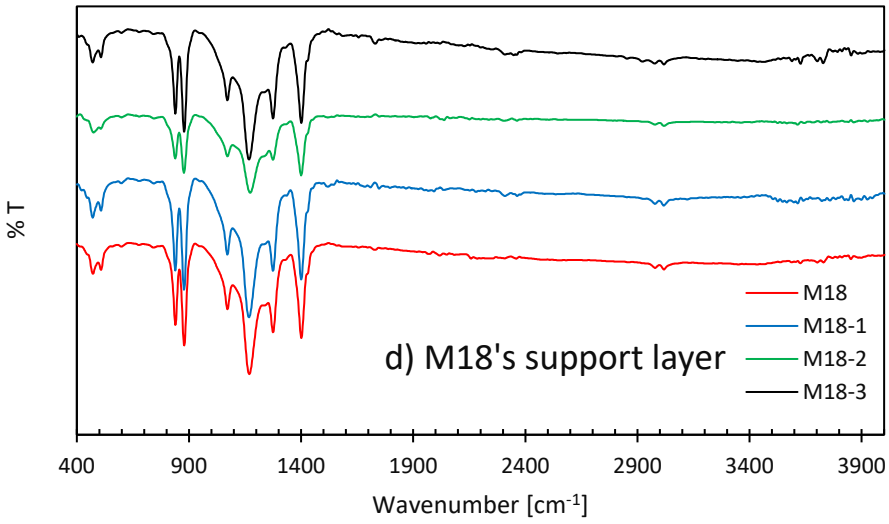

Figure 10 FTIR spectra as a function of SiAG nanoparticle loading (%) on the membrane layers: a) skin layer of M12, b) skin layer of M18, c) sublayer of M12, and d) sublayer of M18

4.7 FTIR Analysis of the Membrane Substrate

As shown in Figure 10c, d the FTIR spectrum of the neat M12 membrane sublayer shows distinct peaks in the range of 840-880 cm-1 and at 1274 cm-1, which confirm the formation of the polymer β phase and a well-defined crystalline structure. Furthermore, the significant intensity of the peak at 474 cm^{-1} may be attributed to the effect of LiCl in creating structural order in the polymer matrix. The detection of peaks related to the –CH2 and –CF2 groups further indicates that the original chemical structure of PVDF is maintained inside the membrane. The FTIR analysis results for the neat M18 sample showed that the peaks observed in the sublayer corresponded to the peaks in the skin layer. This correlation serves as evidence for the stability of the chemical structure of PVDF throughout the membrane thickness and suggests the development of a consistent and orderly structure in both layers. The clear presence of peaks associated with the β phase also indicates the development of polar crystallinity throughout the membrane. The FTIR analysis results indicated that peaks characteristic of the β phase of the PVDF polymer were detected in both the skin layer and the substrate of the M12-1 membrane, demonstrating the preservation of the polar crystalline structure within the membrane. Additionally, the identification of peaks related to Si–O groups in both layers confirms the effective distribution of nanoparticles throughout the membrane's thickness. The distinction in specific surface peaks, specifically at 3727 and 3018 cm^{-1}, is only evident in the skin layer and is likely attributable to surface adsorption or free surface groups linked to the aerogel. In the M18-1 membrane sublayer, the peaks are consistent with the PVDF and presence of LiCl. The lack of a peak in the OH region indicates that the sublayer exhibits hydrophobic characteristics relative to the skin layer, which is consistent with the lower contact angle observed between the skin layer and the substrate. The decrease intensity of the peaks corresponding to polar groups such as $–CF_2$ and $–CH_2$ in the

M12-2 membrane substrate indicates that its surface is less polar compared to the skin layer, leading to reduced hydrophilicity and an increased contact angle. The FTIR peaks in the M18-2 membrane sublayer, especially the peaks associated with the PVDF index, are more prominent. This may indicate that the polymer structure in this layer is more organized and potentially less affected by nanoparticles. The peak at 3018 in the skin layer indicates the potential formation of new bonds that are not present in the sublayer. The intensity of the peaks in the skin layer of the M12-3 membrane is marginally higher than that of the sublayer, especially in the CF_2 and CH_2 regions, indicating higher molecular order or improved aggregation of polymer chains at the active surface. The Si–O peak in both layers is significant (81 and 84), indicating the adequate presence of silica aerogel nanoparticles in the structure of both layers. Nevertheless, the substrate contact angle is higher than the skin layer contact angle, which may be attributed to the tendency of nanoparticles to migrate backward during the phase inversion process (NIPS) or to their non-uniform distribution within the sublayer. The active surface is in direct contact with air, and the rapid evaporation of the solvent can prevent the migration of nanoparticles to the surface, whereas the sublayer's interaction while the interaction of the sublayer with the coagulation bath and slower crystallization allows particles to accumulate on the surface [23].

5.0 CONCLUSION

The performance of PVDF-silica aerogel composite membranes in membrane distillation (MD) is governed by a complex interplay between polymer concentration and nanoparticle loading, which collectively determine critical structural and functional properties. Our findings demonstrate that PVDF concentration dominates porosity response, where higher concentrations (21%) increase solution viscosity, delay phase separation, and reduce porosity, while lower concentrations (12%) allow silica aerogel to enhance porosity. At 18% PVDF, porosity remains stable with nanoparticle loading, striking an optimal balance. The incorporation of silica aerogel drives key functional improvements: it reduces thermal conductivity (beneficial for minimizing conductive heat loss), increases pore size (though this may elevate wetting risk by reducing liquid entry pressure), and preferentially migrates to the sublayer during membrane formation, significantly boosting sublayer hydrophobicity (up to 130° contact angle) without altering the underlying PVDF chemistry. The 18% PVDF/3% silica aerogel membrane emerged as the top performer, combining high sublayer hydrophobicity, structural stability, suitable porosity, and low thermal conductivity. This underscores that optimal membrane design requires synergistic tuning of polymer-nanoparticle ratios rather than simply maximizing individual components. In summary, effective MD membranes demand careful optimization of polymer matrix concentration and additive loading to simultaneously achieve the necessary structural integrity, surface properties, porosity, and thermal insulation—a balance critical for advancing MD technology.

ACKNOWLEDGEMENTS

This research was conducted with the support of the SMTRG at Persian Gulf University. I am especially grateful to

the contributions of our lab assistants, Mrs Malyi for her diligent efforts in thermal conductivity data collection. This study was funded by the National Agriculture Organization of Bushehr Province.

CONFLICTS OF INTEREST

The author(s) declare(s) that there is no conflict of interest regarding the publication of this paper.

REFERENCES

[1] Service, R. F. (2004). *Nanotechnology grows up*. American Association for the Advancement of Science.

[2] Xiang, J., Zhang, L., Li, W., Zhang, H., & Li, J. (2023). Study on low thermal-conductivity of PVDF@SiAG/PET membranes for direct contact membrane distillation application. *Membranes, 13*(9), 773. https://doi.org/10.3390/membranes13090773.

[3] Gontarek-Castro, E., & Castro-Muñoz, R. (2024). How to make membrane distillation greener: A review of environmentally friendly and sustainable aspects. *Green Chemistry*. https://doi.org/10.1039/D4GC01136A.

[4] Shirazi, M. M. A., & Kargari, A. (2015). A review on applications of membrane distillation (MD) process for wastewater treatment. *Journal of Membrane Science and Research, 1*(3), 101–112.

[5] Chen, X., Zhang, Y., Wang, D., Li, J., & He, G. (2018). Tubular hydrophobic ceramic membrane with asymmetric structure for water desalination via vacuum membrane distillation process. *Desalination, 443*, 212–220.

[6] Ali, A., Ong, Y. K., Chung, T. S., & Lai, S. O. (2019). A comparative analysis of flat sheet and capillary membranes for membrane distillation applications. *Desalination, 456*, 1–12.

[7] Nthunya, L. N., Derese, S., Mhlanga, S. D., & Mamba, B. B. (2020). f-MWCNTs/AgNPs-coated superhydrophobic PVDF nanofibre membrane for organic, colloidal, and biofouling mitigation in direct contact membrane distillation. *Journal of Environmental Chemical Engineering, 8*(2), 103654.

[8] Rezaei, M., Hashemifard, S. A., & Abbasi, M. (2022). On performance of polycarbonate/silica aerogel nanoparticle mixed matrix hollow fiber membrane coated with polydimethylsiloxane for membrane distillation. *Journal of Applied Polymer Science, 139*(31), e52719.

[9] Wang, K. Y., Foo, S. W., & Chung, T.-S. (2009). Mixed matrix PVDF hollow fiber membranes with nanoscale pores for desalination through direct contact membrane distillation. *Industrial & Engineering Chemistry Research, 48*(9), 4474–4483.

[10] Qtaishat, M., Matsuura, T., Kruczek, B., & Khayet, M. (2008). Heat and mass transfer analysis in direct contact membrane distillation. *Desalination, 219*(1–3), 272–292.

[11] Gryta, M., Tomaszewska, M., & Karakulski, K. (2006). Wastewater treatment by membrane distillation. *Desalination, 198*(1–3), 67–73.

[12] Li, Z., Wang, X., Zhang, Y., &

Zhang, L. (2014). Effects of thermal efficiency in DCMD and the preparation of membranes with low thermal conductivity. *Applied Surface Science, 317*, 338–349.

[13] Lee, E.-J., Deka, B. J., & An, A. K. (2019). Reinforced superhydrophobic membrane coated with aerogel-assisted polymeric microspheres for membrane distillation. *Journal of Membrane Science, 573*, 570–578.

[14] Zhang, L.-Z., & Su, Q.-W. (2018). Performance manipulations of a composite membrane of low thermal conductivity for seawater desalination. *Chemical Engineering Science, 192*, 61–73.

[15] Deka, B. J., Lee, E.-J., & An, A. K. (2019). Electrospun nanofiber membranes incorporating PDMS-aerogel superhydrophobic coating with enhanced flux and improved antiwettability in membrane distillation. *Environmental Science & Technology, 53*(9), 4948–4958.

[16] Zhang, H., Zhang, L., Zhang, J., Li, J., & Wang, Y. (2018). SiO_2-PDMS-PVDF hollow fiber membrane with high flux for vacuum membrane distillation. *Desalination, 429*, 33–43.

[17] Efome, J. E., Rana, D., Matsuura, T., & Lan, C. Q. (2015). Effects of superhydrophobic SiO_2 nanoparticles on the performance of PVDF flat sheet membranes for vacuum membrane distillation. *Desalination, 373*, 47–57.

[18] Li, K., Zhang, X., Wang, Y., Zhang, L., & Li, J. (2020). A polyvinylidene fluoride (PVDF)–silica aerogel (SiAG) insulating membrane for improvement of thermal efficiency during membrane distillation. *Journal of Membrane Science, 597*, 117632.

[19] Lovineh, S. G., Asghari, M., & Rajaei, B. (2013). Numerical simulation and theoretical study on simultaneous effects of operating parameters in vacuum membrane distillation. *Desalination, 314*, 59–66.

[20] Naim, R., & Ismail, A. (2013). Effect of polymer concentration on the structure and performance of PEI hollow fiber membrane contactor for CO_2 stripping. *Journal of Hazardous Materials, 250*, 354–361.

[21] Khalifa, A., Ahmed, M., & Osman, A. (2017). Experimental and theoretical investigations on water desalination using direct contact membrane distillation. *Desalination, 404*, 22–34.

[22] Adnan, S., Johnson, D., Hilal, N., & Francis, L. (2012). Commercial PTFE membranes for membrane distillation application: Effect of microstructure and support material. *Desalination, 284*, 297–308.

[23] Huang, Z., Liu, Z., Li, L., Liu, J., & Zhang, Y. (2021). Dual-layer membranes with a thin film hydrophilic MOF/PVA nanocomposite for enhanced antiwetting property in membrane distillation. *Desalination, 518*, 115268.